Journal of Sound and Vibration (2001) **248**(1), 123–149
doi:10.1006/jsvi.2001.3770, available online at http://www.idealibrary.com on IDEAL®

ON THE PREDICTION OF "BUZZ-SAW" NOISE IN AERO-ENGINE INLET DUCTS

A. McAlpine and M. J. Fisher

Institute of Sound and Vibration Research, University of Southampton, Southampton SO17 1BJ, England. E-mail: am@isvr.soton.ac.uk

(*Received* 8 *August* 2000, *and in final form* 5 *April* 2001)

"Buzz-saw" noise radiated from an aero-engine inlet duct occurs when the relative speed of the inlet flow impinging on the fan blades is supersonic. The pressure field attached to a supersonic ducted fan, in a direction normal to the shock fronts, closely resembles a sawtooth waveform. The non-linear propagation of a high-amplitude sawtooth waveform spiralling around a duct is calculated by two numerical simulation models. The models and their validation are discussed critically. Results are presented comparing the numerical simulations with experimental data. Overall there is good agreement comparing the results of the simulations with the experimental data, and in particular, the "Buzz-saw" noise in a hard-walled aero-engine inlet duct is successfully predicted.

1. INTRODUCTION

Entry into service in the 1970s of higher bypass ratio aircraft engines led to the emergence of an additional noise source generated by aircraft engine fans. The prevalent noise sources from earlier generations of aircraft engine fans were commonly divided into two categories: tonal and broadband noise. Tonal noise is generated by rotor–stator interactions and is typically a high pitched "shrill whine", with a corresponding frequency spectrum characterized by energy at harmonics of the fan blade passing frequency. Broadband noise is usually generated by flow turbulence and random vortex shedding.

The new aircraft engines now operate with fan tip speeds exceeding sonic velocity. This generates tones with frequencies at multiples of the engine shaft rotation frequency. This noise source has been referred to as "combination", "multiple pure" or "Buzz-saw" tones; the latter because (allegedly) the sound is similar to that of a circular buzz-saw. The subjective quality of the "Buzz-saw" noise will be more "ragged", and at a lower pitch, than the tonal noise heard from a fan operating at subsonic conditions.

"Buzz-saw" noise is particularly apparent during take-off and climb, and affects both the cabin and community noise levels. With the continual growth in commercial air traffic, in addition to increased public expectations regarding noise levels, the prediction and control of aircraft engine noise emissions remains an important factor in their design. Whilst the majority of research on "Buzz-saw" noise appears to have been during the early 1970s, the problem remains of practical interest because of the design of newer and larger engines, and increasingly stringent noise requirements.

The generation of "Buzz-saw" noise has been addressed by several authors in the 1970s including: Philpot in 1970 [1]; Hawkings, Kurosaka, Fink all in 1971 [2–4]; Pickett in 1972 [5] and Stratford and Newby in 1977 [6]. At this time the mechanism (described below) generating "Buzz-saw" noise was reasonably well understood by these authors.

0022-460X/01/460123 + 27 $35.00/0

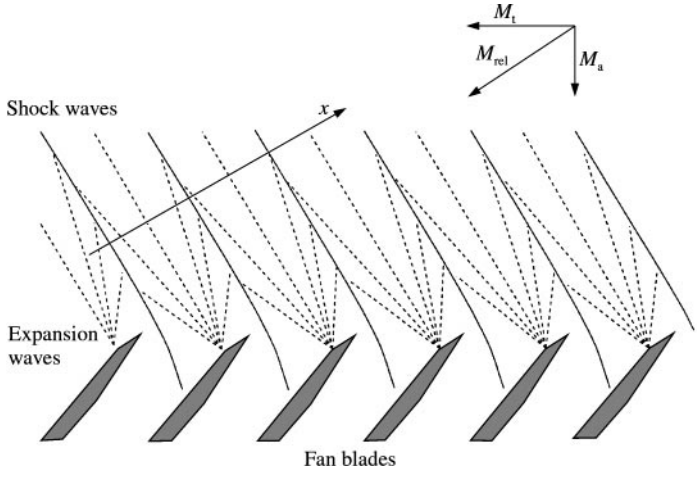

Figure 1. Shock-wave generation by a supersonic fan.

A simple plane two-dimensional model of the "rotor-alone" pressure field, with supersonic flow impinging on the fan rotor blades, is shown in Figure 1. For this model it is assumed that the approach flow is uniform (no inlet guide vanes), weak-shock theory is applicable and that dissipative effects due to viscosity and heat conduction are neglected. The Mach numbers of the approach flow and fan blade tips are M_a and M_t respectively. This results in a flow impinging on the rotor blades with relative Mach number M_{rel}.

For $M_{rel} > 1$ the pressure field consists of a series of bow shock waves and Prandtl–Meyer expansion fans. The expansion fans facilitate turning of the flow onto the suction surface of each rotor blade. The pressure signature in a direction normal to the shock fronts will resemble a sawtooth once the shock waves and expansion fans have coalesced into a continuous waveform, which is assumed to occur shortly upstream of the fan.

The pressure signature associated with an ideal fan, consisting of precisely identical rotor blades in a uniform flow, will be a regular sawtooth (Figure 2(a)). The frequency spectrum of a regular sawtooth (Figure 2(b)) only contains energy at the blade passing frequency (BPF) harmonics. All the shocks propagate upstream of the fan at the undisturbed speed of sound a_0 relative to the oncoming fluid (weak-shock theory), and therefore the blade-to-blade periodicity in the pressure signature is maintained. Thus, the pressure signature remains a regular sawtooth, with shock strength that decays asymptotically as z^{-1}, where z is the axial distance upstream of the fan. Figure 3 shows the resulting pressure signature (and frequency spectrum) on propagating this regular sawtooth over the length of a typical inlet duct. The energy remains at the BPF harmonics, and therefore high-pitched tonal noise (predominantly at BPF) is predicted to be radiated from the inlet of an ideal fan.

In practice, the rotor blades will not be precisely identical; there will be small variations between the blades' profiles, spacings and stagger angles. Hence, the pressure signature will be an irregular sawtooth (Figure 4(a)) which contains features that repeat only once per engine revolution. The frequency spectrum of an irregular sawtooth (Figure 4(b)) now contains energy distributed amongst harmonics based on the engine rotation frequency $\mathscr{F}$, namely Engine Orders (EO).

Shortly upstream of the fan the dominant energy is still at the BPF harmonics (Figure 4(b)). The shocks in an irregular sawtooth will propagate upstream of the fan at slightly different speeds, and therefore the shocks in the sawtooth will become increasingly

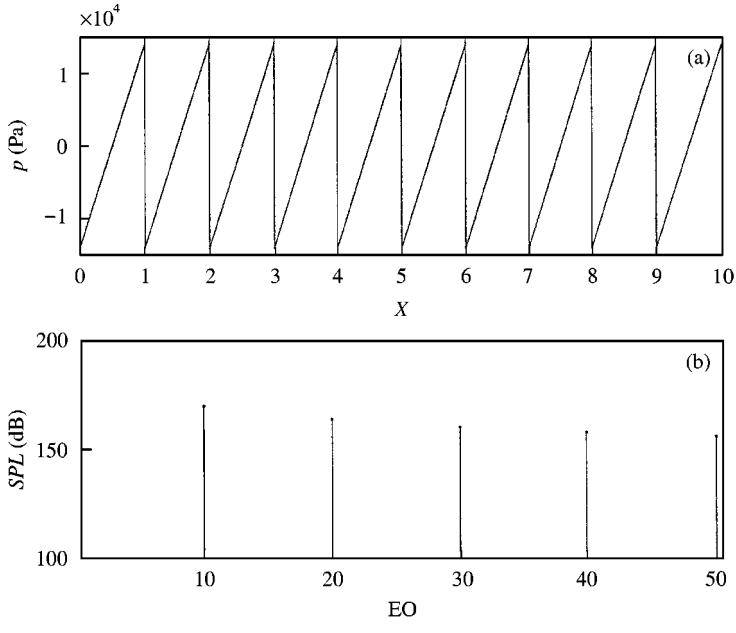

Figure 2. Example of a regular sawtooth generated by an ideal fan (with 10 rotor blades): (a) pressure signature and (b) frequency spectrum.

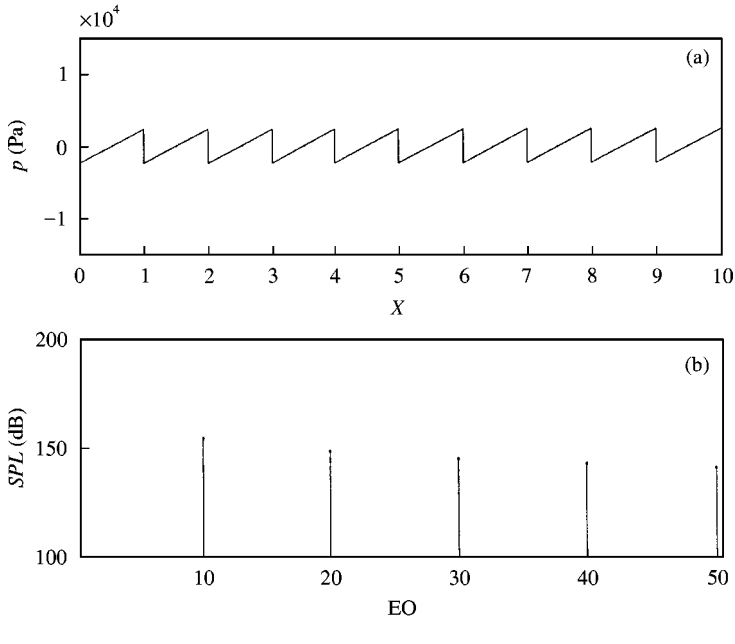

Figure 3. Example of a regular sawtooth located near the end of the inlet duct: (a) pressure signature and (b) frequency spectrum.

non-uniformly spaced. On propagating this irregular sawtooth over the length of a typical inlet duct, the resulting pressure signature (and frequency spectrum) is shown in Figure 5. The blade-to-blade periodicity observed in the pressure signature near the fan has been lost, and the dominant energy is now at EO harmonics whose frequencies are less than BPF. The

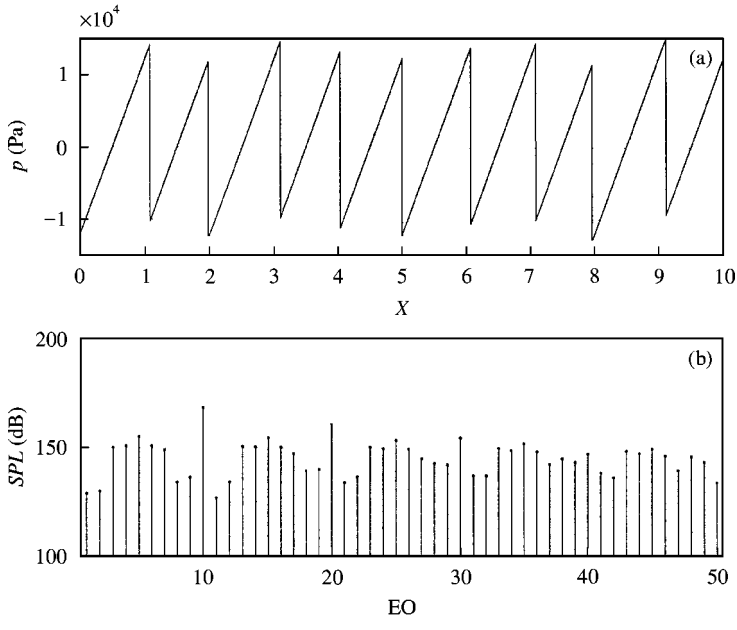

Figure 4. Example of an irregular sawtooth generated by a non-ideal fan (with 10 rotor blades): (a) pressure signature and (b) frequency spectrum.

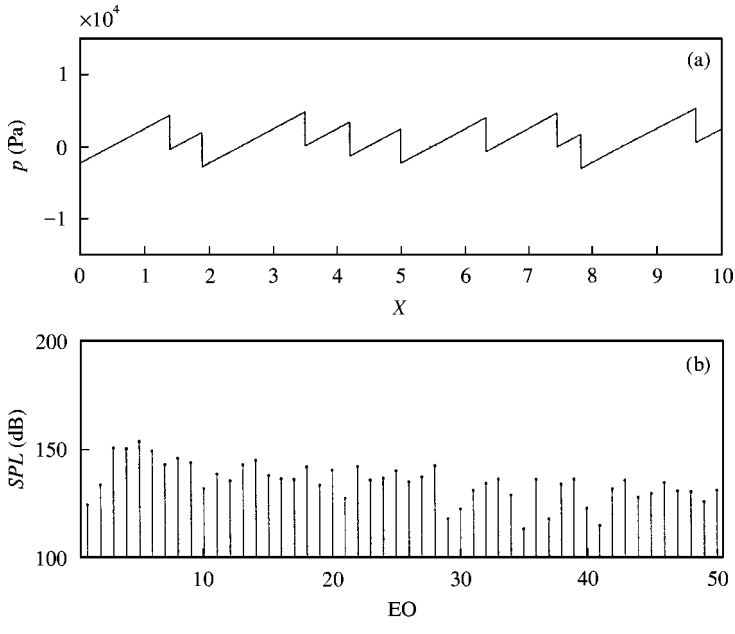

Figure 5. Example of an irregular sawtooth located near the end of the inlet duct: (a) pressure signature and (b) frequency spectrum.

redistribution of acoustic energy between the EO harmonics occurs during the non-linear propagation of a high-amplitude irregular sawtooth pressure waveform. The non-linear propagation of a regular sawtooth only redistributes acoustic energy between the BPF harmonics. Therefore, a lower-pitched more "ragged" noise is predicted to be radiated from

the inlet of a non-ideal fan because of the presence of energy in the low-frequency EO harmonics.

The EO harmonics are spinning modes which are all steady in a frame of reference rotating with the rotor/fan. Hence, in this paper the EO harmonics (including the BPF harmonics) are defined as the "rotor-alone" tones, whereas the "Buzz-saw" tones are defined as the EO harmonics with frequency less than BPF. The characteristic "Buzz-saw" signature of a supersonic fan will resemble Figure 5(b) with the dominant acoustic energy at frequencies less than BPF.

Stratford and Newby considered the sources of blade non-uniformities, and suggested that the initial variations in shock strength are largely attributable to stagger angle variations of $\mathcal{O}(0{\cdot}1^\circ)$. They proposed that the shock detachment distance (from the fan's leading edge), controls the variation in shock strength observed near the fan. This distance depends upon the amount of flow spillage between neighbouring blade passages, and is predominantly affected by variations in the blade stagger angle.

In this paper, two numerical simulation models are used to calculate the non-linear propagation of an irregular sawtooth which traces out a helical path as the waveform spirals around the duct. It is assumed that the flow is only supersonic at a radial location close to the rotor blade tips. Then, a sawtooth waveform spiralling upstream in an inlet duct will be confined to a nominally fixed radial location "close" to the duct wall. This waveform will be steady in a frame of reference rotating with the rotor/fan, and therefore is defined as the "rotor-alone" pressure field. With increasingly high tip speeds there will be supersonic flow over more of the blade span, and it is anticipated that three-dimensional effects will become significant. However, for all the operating conditions studied in this paper the radial extent of supersonic flow over the blade span will be confined to a small region close to the rotor blade tips.

Morfey and Fisher in 1970 [7] calculated the non-dimensional "time of flight" T of a wave spiralling around a duct in terms of the axial distance upstream of the fan z:

$$T = a_0 t/\lambda = (z/D)K, \tag{1}$$

where

$$K = \frac{B}{\pi}\frac{M_{rel}^4}{\sqrt{M_{rel}^2 - 1}}\left(M_a\sqrt{M_{rel}^2 - 1} - M_t\right)^{-2} \tag{2}$$

and λ is the inter-shock spacing (m), B is the number of fan blades and D is the duct diameter (m).

Morfey and Fisher also calculated the non-linear attenuation of a regular sawtooth in terms of the "time of flight" T. By using the weak-shock theory, the velocity v of a point on a pressure waveform is calculable in terms of the pressure p at that point. Similarly, the velocity of a shock front v_s is calculable in terms of the amplitude of the shock mid-point pressure p_m. Thus,

$$v(p) = a_0 + \frac{\gamma + 1}{2\rho_0 a_0}p, \qquad v_s(p_m) = a_0 + \frac{\gamma + 1}{2\rho_0 a_0}p_m, \tag{3, 4}$$

where the pressure p is the deviation from the mean static pressure P_0, γ is the adiabatic constant, and ρ_0 the mean density.

For a regular sawtooth the attenuation on the high- and low-pressure sides of each shock will therefore be equal, and the waveform will maintain it's shape during propagation. The

non-linear attenuation of a regular sawtooth is given by

$$p_s(T) = \frac{P_0 s}{1 + \left(\frac{\gamma + 1}{2\gamma}\right) Ts}, \tag{5}$$

where p_s is the amplitude of the shock and $s = p_s(0)/P_0$ is the (non-dimensional) starting shock strength. When $Ts \gg 1$ equation (5) reduces to

$$p_s(T) \approx \left(\frac{2\gamma P_0}{\gamma + 1}\right) \frac{1}{T} \tag{6}$$

with a shock strength p_s now independent of the starting shock strength s. This suggests that for a regular sawtooth a reasonable prediction of the shock strength at the end of the duct may be obtained without a precise knowledge of the shock properties near the fan.

The non-linear propagation of shock waves upstream of a supersonic fan will be calculated in terms of T in each of the simulation models discussed in this paper. This simplifies the problem because T is dependent upon the operating conditions (M_a and M_t), as well as the number of rotor blades B and the diameter of the duct D (cf. equations (1) and (2)). Therefore, changes in any of these parameters may simply be related to a change in T.

In section 2, the prediction of the non-linear propagation of an irregular sawtooth is considered. Two alternative simulation models are discussed. The acronyms Time Domain Numerical Solution (TDNS) and Frequency Domain Numerical Solution (FDNS) are introduced in order to identify the non-linear propagation models described in sections 2.1 and 2.2 respectively. (The identifying names TDNS and FDNS reflect the spirit in which each of these models were developed.)

The non-linear propagation of an irregular sawtooth is calculable in the time domain. The first model (TDNS) was described by Fisher *et al.* in 1998 [8], and is similar to a method described by Hawkings in 1971 [2]. Brief results of Fisher *et al.* suggested that the BPF tone in a hard-walled inlet duct may be predicted reasonably well by using TDNS. In this paper, spectral comparisons between numerical simulations and experimental data will also be included.

Fisher *et al.* recognized that the applicability of using TDNS is limited to hard-walled inlet ducts. In practice, most inlet ducts on modern aero-engines have an acoustic liner on the duct wall (i.e., a soft-walled duct). Therefore, Fisher *et al.* proposed an alternative simulation model, FDNS, in which the problem is transformed into the modal/frequency domain in order to include (approximately) the effect of an acoustic duct liner.

In this paper, the FDNS model is developed further from the original model proposed by Fisher *et al.* It is anticipated that the model will be used primarily for noise predictions with soft-walled inlet ducts. However, in hard-walled inlet ducts the "cut-off" phenomenon may also be included in FDNS. Results in this paper are confined to comparisons with experimental data obtained in a hard-walled inlet duct. These show that by using FDNS the EO frequency spectrum measured in the inlet duct at axial stations upstream of the fan may be reasonably well predicted. In particular, the "Buzz-saw" tones are closely predicted by the numerical simulation. In a hard-walled inlet duct FDNS provides a significant improvement over TDNS because of the inclusion of "cut-off" in the model.

The FDNS model derived in section 2.2 is in theory applicable to both hard- and soft-walled inlet ducts. In a subsequent paper, the applicability of using FDNS with a soft-walled inlet duct will be discussed.

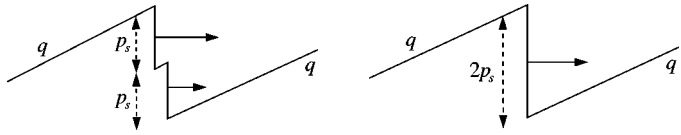

Figure 6. Shock merging.

2. NON-LINEAR PROPAGATION MODELS

The non-linear attenuation of a regular sawtooth predicted by equation (5) (or approximately by equation (6)) provides a simple analytic expression for the decay of the BPF tone in a hard-walled inlet duct. However, the generation and subsequent non-linear propagation of harmonics of the engine rotation frequency, i.e., EO harmonics, are not included in the regular sawtooth model.

In this section, two numerical simulation models are outlined which predict the non-linear propagation of an irregular sawtooth spiralling upstream in an inlet duct. The first model (TDNS) calculates the non-linear propagation of a sawtooth waveform in the time domain. The second model (FDNS) expresses a sawtooth waveform in terms of a summation of Fourier harmonics (equivalent to the EO harmonics). The attenuation of each harmonic is then calculated by integrating a series of coupled differential equations.

The initial construction of an irregular sawtooth resembling the pressure signature close to the fan in an inlet duct is discussed later in section 3.2.

2.1. TDNS MODEL

The non-linear propagation of an irregular sawtooth is calculable in the time domain by using the weak-shock theory in equations (3) and (4) because these specify the velocity of each point on the waveform. In TDNS, an irregular sawtooth is constructed (nominally located at a small distance upstream of the fan), and then the waveform's propagation is calculated in the time domain, which may be simply translated into axial distance z upstream of the fan by using equation (1).

The shocks propagate at different velocities, and therefore at some point two (or more) shocks may merge. Figure 6 sketches two shocks merging. The expansion fan gradient q remains unaltered; however, the new shock's amplitude will equal $2p_s$, with a mid-point pressure equal to the average of the mid-point pressures of the two shocks which have merged.

Further details about the TDNS model are described by Fisher *et al*. Currently, TDNS is written in MatLab, and the run-time (over a typical duct length) is about 60 s on a modern PC. Hence, it is an extremely useful model to use to run a large number of simulations in a short time period.

The plane two-dimensional model of the "rotor-alone" pressure field does not include the inlet duct wall. Therefore, this planar model compared with the inlet duct (sketched in Figure 7) may be thought of as equivalent to a model without the inclusion of the radial dependence r. In order to include the effect of "cut-off" (hard-walled duct) or liner performance (soft-walled duct), it is required to transform the problem into the modal/frequency domain, because "cut-off" and liner performance are determined by mode number and frequency. This may not be easily incorporated into the time domain.

2.2. FDNS MODEL

Consider a cylindrical inlet duct containing a uniform axial flow with Mach number M_a, and take cylindrical polar co-ordinates (r, θ, z) such that the centre of the duct is aligned with the z-axis, and the duct wall is at $r = b$ (cf. Figure 7).

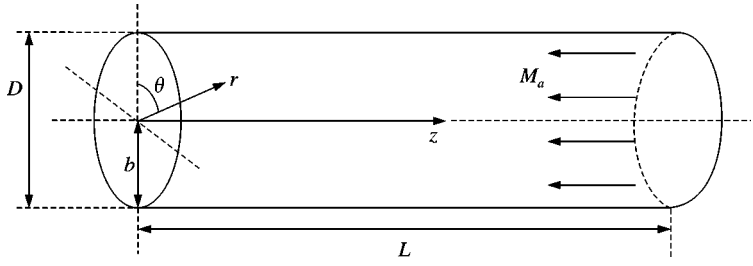

Figure 7. Cylindrical inlet duct.

Assume that a harmonic noise source (with frequency ω) is introduced into the duct, resulting in a harmonic pressure field $p(r, \theta, z, t) = \hat{p}(r, \theta, z)\exp(\mathrm{i}\omega t)$ which satisfies the convected Helmholtz equation

$$\left(\mathrm{i}k + M_a \frac{\partial}{\partial z}\right)^2 \hat{p} = \nabla^2 \hat{p}, \tag{7}$$

where $k = \omega/a_0$.

It is well known (e.g., as shown by Eversman [9]) that on separating the variables r, θ and z a modal solution of equation (7) will be of the form

$$\hat{p}_{mn}(r, \theta, z) = A_{mn} \mathrm{J}_m(\kappa_{mn} r)\exp[\mathrm{i}(-k_z z \pm m\theta)], \tag{8}$$

where

$$k_z = \frac{k}{1 - M_a^2}\left[-M_a \pm \left\{1 - (1 - M_a^2)\left(\frac{\kappa_{mn}}{k}\right)^2\right\}^{1/2}\right], \tag{9}$$

m and n are integers, A_{mn} is a constant and J_m is the Bessel function of the first kind of order m. Modal solution (8) has azimuthal and axial wavenumber m and k_z, respectively, and radial eigenvalues denoted by κ_{mn}.

The boundary condition for a duct with a locally reacting wall with (non-dimensional) specific acoustic impedance Z reduces to the following eigenvalue problem:

$$\kappa_{mn} b \frac{\mathrm{J}'_m(\kappa_{mn} b)}{\mathrm{J}_m(\kappa_{mn} b)} = -\mathrm{i}kbA\left(1 - M_a \frac{k_z}{k}\right)^2, \tag{10}$$

where $A = 1/Z$ is the specific acoustic admittance. In a hard-walled inlet duct $A \equiv 0$ and equation (10) reduces to

$$\mathrm{J}'_m(\kappa_{mn} b) = 0, \tag{11}$$

where the radial eigenvalue κ_{mn} denotes the nth turning point of the Bessel function J_m.

In a hard-walled inlet duct a mode is said to be "cut-off" when k_z is complex. A "cut-off" mode decays exponentially, and from equation (8) has the form

$$\hat{p}_{mn}(r, \theta, z) = A_{mn} \mathrm{J}_m(\kappa_{mn} r)\exp[\mathrm{i}(-k_{zr} z \pm m\theta)]\exp(k_{zi} z), \tag{12}$$

where $k_z = k_{zr} + \mathrm{i}k_{zi}$, and it is understood that the sign of the square root in equation (9) is chosen such that $k_{zi} < 0$ for modes propagating in the positive z direction, and $k_{zi} > 0$ for modes propagating in the negative z direction.

The "rotor-alone" pressure field attached to a supersonic† ducted rotor may also be expressed as a superposition of modes; however, in this case, each mode will be steady in the rotor's frame of reference. Therefore, the "rotor-alone" pressure field will consist of a superposition of modes whose angular frequency ω and azimuthal wavenumber m are not independent. The ratio ω/m (circumferential phase velocity) will be constant, and will equal $2\pi\mathscr{F}$. Therefore, the azimuthal wavenumber m is equivalent to the Engine Order (EO).

In general, over the range of operating conditions (i.e., values of M_a and M_t) of a supersonic fan, radial modes with $n \geqslant 2$ will usually be "cut-off". The first radial mode $n = 1$ will also frequently be "cut-off" for the low EO modes, i.e., $m = 1, 2, 3, \ldots$. Therefore, it is plausible that a superposition of only the first order radial modes will give a reasonable approximation to the acoustic pressure field in a cylindrical inlet duct, because the majority of higher order radial modes will be "cut-off". The energy in the first radial mode is distributed largely near the duct wall (because there is a maximum point in the Bessel function at the wall). Thus, a two-dimensional (θ, z) acoustic pressure field, with r constant (and nominally taken to be $r \approx b$) is used to approximate a three-dimensional (r, θ, z) acoustic pressure field in a hard-walled cylindrical inlet duct.

The predicted linear attenuation with axial distance upstream of the fan, for the "cut-off" EO modes is given by

$$|\hat{p}_{mn}| = |\hat{p}_{mn}(z = 0)| \exp(k_{zi} z). \tag{13}$$

The length of the inlet duct for a typical aero-engine (with the fan located at $z = 0$, and the end of the inlet duct at $z = \mathrm{L}$) is $L \approx \frac{1}{2}D$. Therefore, by solving the eigenvalue problem defined by equations (9) and (10), and using equation (13), the linear attenuation per duct length may be predicted for each EO m. The solution of this eigenvalue problem has been discussed by Eversman [9]. In a hard-walled inlet duct, the linear attenuation will only be non-zero for EOs which are "cut-off".

Now define the moving spatial co-ordinate x (with velocity a_0) to be the direction normal to the shock fronts (cf. Figure 1). Then it is well known (e.g., as shown by Crighton [10] and Whitham [11]) that the non-linear propagation of a simple wave may be described by

$$\frac{\partial p}{\partial t} + \frac{\gamma + 1}{2\rho_0 a_0} p \frac{\partial p}{\partial x} = 0. \tag{14}$$

In the book by Crighton *et al.* [12] (see pp. 648–656) the "simple wave equation" (14) is derived from the non-dissipative Euler equations by using the method of multiple scales. Equation (14) is also derived in gas dynamics by using the theory of Riemann Invariants, and therefore equation (14) was referred to as the Riemann equation by Fisher *et al.*

On substituting the non-dimensional variables

$$T = \frac{a_0 t}{\lambda}, \quad X = \frac{2\pi}{B}\frac{x}{\lambda} \quad \text{and} \quad P = \left(\frac{\gamma + 1}{2\gamma}\right)\frac{p}{P_0}, \tag{15}$$

into equation (14), the non-dimensional "simple wave equation" is

$$\frac{\partial P}{\partial T} + \frac{2\pi}{B} P \frac{\partial P}{\partial X} = 0. \tag{16}$$

†These comments also apply to subsonic ducted rotors but the associated modes are always "cut-off" and need not be considered further.

Assuming the weak-shock approximation remains valid, the propagation of a waveform including weak shocks may still be described by equation (16) (cf. the book by Whitham [11], p. 176).

Fisher *et al.* recognized that the effect of an acoustic liner on the attenuation of an irregular sawtooth spiralling around a soft-walled inlet duct may be modelled by transforming equation (16) into the modal/frequency domain. This frequency-domain approach was first suggested by Fenlon [13] in 1971 (and has been implemented by several authors since).

Express the irregular sawtooth in terms of a complex Fourier series

$$P(X, T) = \sum_{m=-\infty}^{\infty} C_m(T) e^{imX}, \tag{17}$$

where $C_{-m} = \tilde{C}_m$ ($\tilde{}$ denotes complex conjugate), and $C_0 \equiv 0$. Then substitute equation (17) into equation (16) to obtain the coupled spectral differential equations:

$$\frac{dC_m}{dT} = -\frac{im\pi}{B}\left(\sum_{l=1}^{m-1} C_{m-l}C_l + 2\sum_{l=m+1}^{\infty} C_l\tilde{C}_{l-m}\right). \tag{18}$$

The "simple wave equation" is a lossless propagation equation; the non-linear term transfers energy between the modes, but there will be no net change in the acoustic energy. It is assumed that dissipation occurs only at the shocks. (In TDNS, it is implicitly assumed that the energy dissipated by the shocks is equal to the loss of energy predicted by the non-linear attenuation of each shock.) Therefore, in order to predict the non-linear attenuation of the shocks by using this lossless propagation equation, the Fourier series representation of the irregular sawtooth may not be truncated. However, on numerically integrating equation (18) it is necessary to truncate the second summation. Thus, a dissipative term is required to be included in this model equation.

The simplest model that describes the combination of non-linearity and dissipation is Burgers equation, which may be written as

$$\frac{\partial P}{\partial T} + \frac{2\pi}{B} P\frac{\partial P}{\partial X} = \frac{\varepsilon}{B^2}\frac{\partial^2 P}{\partial X^2}, \tag{19}$$

in terms of the non-dimensional variables (15). The diffusive term $(\varepsilon/B^2)\partial^2 P/\partial X^2$ is added to the RHS of equation (16) to form Burgers equation. The diffusive term is included to explicitly dissipate energy, particularly at frequencies close to where the infinite summation in equation (18) is truncated. The calculation of a suitable value for ε, which is called here the *dissipation constant*, is described in section 2.3.

Fisher *et al.* suggested the inclusion of a linear attenuation term $-\sigma(m)C_m$ in equation (18), which is mode number (or frequency) dependent, in order to approximate the liner damping. This is effectively an absorption term. (In 1980, Korpel [14] first used coupled spectral equations that included the effect of both absorption and dispersion.)

In a hard-walled inlet duct the inclusion of this linear attenuation term is used to incorporate the effect of "cut-off", whence $\sigma(m) \neq 0 \Leftrightarrow$ EO m is "cut-off". The modified coupled spectral differential equations (with the inclusion of the numerical dissipation term and the linear attenuation term) are now:

$$\frac{dC_m}{dT} = -\frac{im\pi}{B}\left(\sum_{l=1}^{m-1} C_{m-l}C_l + 2\sum_{l=m+1}^{N} C_l\tilde{C}_{l-m}\right) - \varepsilon\frac{m^2}{B^2}C_m - \sigma(m)C_m. \tag{20}$$

The linear attenuation rate $\sigma(m)$ is dependent upon mode number (or frequency), and is calculated by setting

$$\sigma(m) = \mathrm{Re}\left\{\frac{\mathrm{i}k_z D}{K}\right\} = -\frac{k_{zi} D}{K}, \tag{21}$$

where k_z is the axial wavenumber for the $(m, 1)$ duct mode, and K is defined by equation (2).

In order to initiate this calculation one needs a waveform at an arbitrary position ($T \approx 0$) upstream of the fan from which an initial set of Fourier coefficients may be determined. This may be obtained from a CFD calculation, for example, or determined from acoustic measurements near the fan as described in section 3.2. Subsequently, one proceeds to successive axial stations in the duct finding the new Fourier coefficients C_m by integrating equation (20) using a fourth order Runge–Kutta numerical integration scheme. The Fourier series is truncated at the $m = N$th term. Currently, FDNS is written in FORTRAN, and by choosing a suitable value for the dissipation constant (say $\varepsilon = \varepsilon_c$), the number of terms required in the Fourier series is typically $N = 100 \times B$. Then the run-time (over a typical duct length) is about 1 hr on a modern PC.

The non-linear spectral interactions may be analyzed by close inspection of equation (20). The non-linear terms $C_{m-l}C_l$ and $C_l\tilde{C}_{l-m}$ describe the transfer of energy between the modes. Non-linear interactions affecting the energy in the mth mode occur between modes whose mode numbers either sum ($C_{m-l}C_l$), or difference ($C_l\tilde{C}_{l-m}$), to the value m.

In a regular sawtooth the BPF harmonics are attenuated by the transfer of energy to higher frequency BPF harmonics (where the higher frequencies are more efficiently dissipated by the shocks). The diffusive term in Burgers equation is proportional to m^2, and therefore the higher frequencies will be more efficiently dissipated by this model equation.

In theory, when $P \ll 1$ (i.e., linear acoustics) equation (20) should reduce to

$$\frac{\mathrm{d}C_m}{\mathrm{d}T} = -\sigma(m)C_m, \tag{22}$$

$$\Rightarrow |C_m| = |C_m(T = 0)| \exp(-\sigma T) \tag{23}$$

with equation (23) equivalent to equation (13). However, equation (20) reduces to

$$\frac{\mathrm{d}C_m}{\mathrm{d}T} = -\left(\varepsilon\frac{m^2}{B^2} + \sigma(m)\right)C_m. \tag{24}$$

In FDNS, when $P \ll 1$ there will be too much numerical dissipation in the model. However, in the frequency range of interest (which will typically be up to about 4 or $5 \times$ BPF) the diffusive term is small compared with its size at the higher frequencies The amount of dissipation required in the FDNS model (i.e., the size of the dissipation constant ε) is directly related to the number of Fourier harmonics N to be calculated, and the accuracy required. With a regular sawtooth it is demonstrated in section 2.3 that by setting $N = 100 \times B$ the FDNS model accurately predicts the Sound Pressure Level (SPL) up to at least $5 \times$ BPF, over a distance greater than the length of a typical inlet duct.

2.3. VALIDATION OF THE FDNS MODEL

First, the FDNS model is validated by comparison with the theory for a regular sawtooth. By using the theory for a regular sawtooth as a basis for the FDNS model, a suitable dissipation constant $\varepsilon = \varepsilon_c$ is found. It is presumed that the amount of dissipation

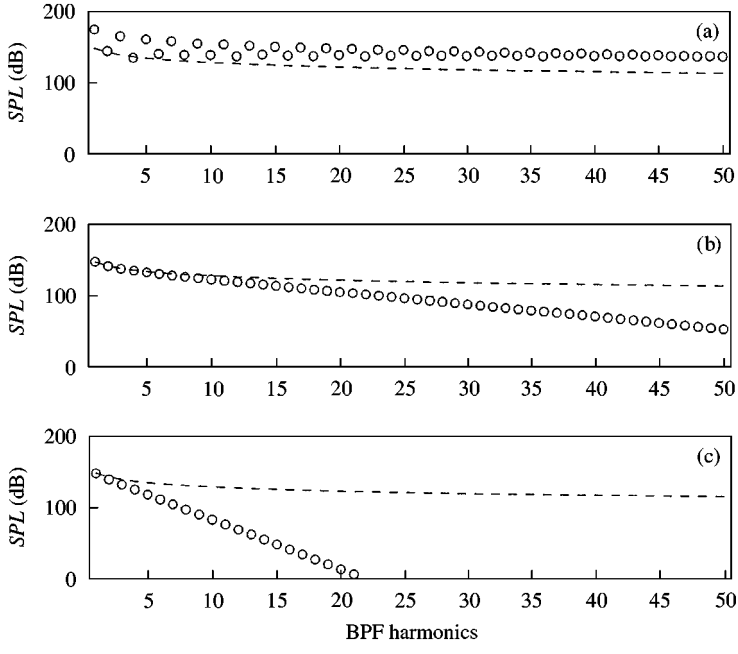

Figure 8. FDNS: BPF harmonics 1–50, (a) $\varepsilon < \varepsilon_c$, (b) $\varepsilon = \varepsilon_c$ and (c) $\varepsilon > \varepsilon_c$. Comparison between the theory for a regular sawtooth and FDNS results on propagating a regular sawtooth waveform over the length of a typical inlet duct: – – –, regular sawtooth; ○, FDNS.

required for a regular sawtooth will be of the same order for an irregular sawtooth, and the comparison between TDNS and FDNS results to be reviewed later in this paper (Figures 11 and 12) supports this assumption.

The amount of dissipation introduced into the model depends upon the number of Fourier harmonics N to be calculated, and the accuracy required. Figure 8 demonstrates the effect of calculating the BPF harmonics for a regular sawtooth by using three different values of the dissipation constant (and setting $N = 100 \times B$). Figure 8(a) demonstrates the effect of too little dissipation in the model. Energy is transferred to the high frequencies and harmonics close to the truncation point gain energy which is not dissipated. This leads to poor agreement with the theory for a regular sawtooth over the entire frequency range. Figure 8(b) shows that with $\varepsilon = \varepsilon_c$ it is possible to match approximately the first 10 BPF harmonics with the theory (by calculating up to the 100th BPF harmonic). Finally, Figure 8(c) demonstrates the effect of too much dissipation in the model. A comparison of the lower BPF harmonics in Figure 8(b) and 8(c) shows that too much dissipation has little effect on the first BPF harmonic. Therefore, in this model the effect of too much dissipation is preferable as opposed to too little. Typically, one can analyze the results up to the fourth BPF harmonic, and provided there is a sufficient amount of dissipation in the model, the precise amount does not need to be determined exactly.

Figure 9 shows BPF harmonics 1–4, and Figure 10 BPF harmonics 5, 10, 15 and 20, against the prediction for a regular sawtooth. There is good agreement up to between the 5th and the 10th BPF harmonic. It is assumed that although the higher BPF harmonics are necessarily dissipated more rapidly than is predicted for a regular sawtooth (because the Fourier series is truncated), non-linear interactions between these very high frequencies do not significantly affect the lower frequencies within the range of interest.

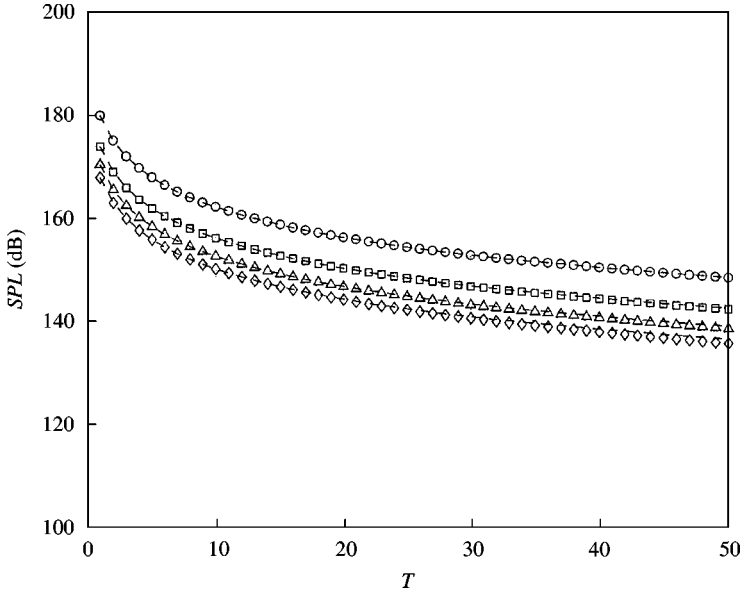

Figure 9. FDNS: BPF harmonics 1–4. Comparison between the theory for a regular sawtooth and FDNS results: – – –, regular sawtooth; ○, 1 × BPF; □, 2 × BPF; △, 3 × BPF; ◇, 4 × BPF.

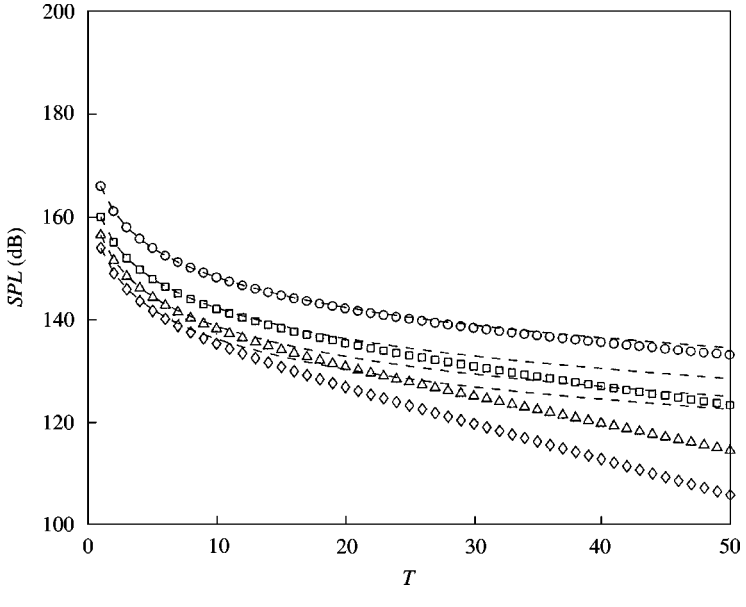

Figure 10. FDNS: BPF harmonics 5–20. Comparison between the theory for a regular sawtooth and FDNS results: – – –, regular sawtooth; ○, 5 × BPF; □, 10 × BPF; △, 15 × BPF; ◇, 20 × BPF.

Secondly, results between TDNS and FDNS are compared (on setting $\sigma \equiv 0$ in equation (20)), to validate the use of Burgers equation when modelling the non-linear propagation of an irregular sawtooth. This comparison is also used to demonstrate the limitation of TDNS; namely that the evanescent decay of the "cut-off" modes is not included in this model.

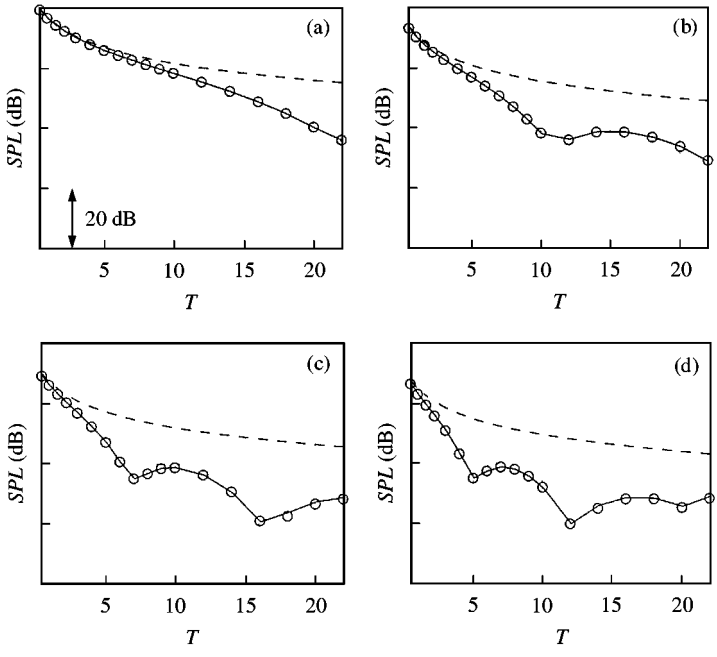

Figure 11. TDNS/FDNS: BPF harmonics 1–4. Comparison between TDNS results and FDNS results for an example of an irregular sawtooth: – – –, regular sawtooth; ——, TDNS; ○, FDNS. (a) 1BPF; (b) 2BPF; (c) 3BPF; (d) 4BPF.

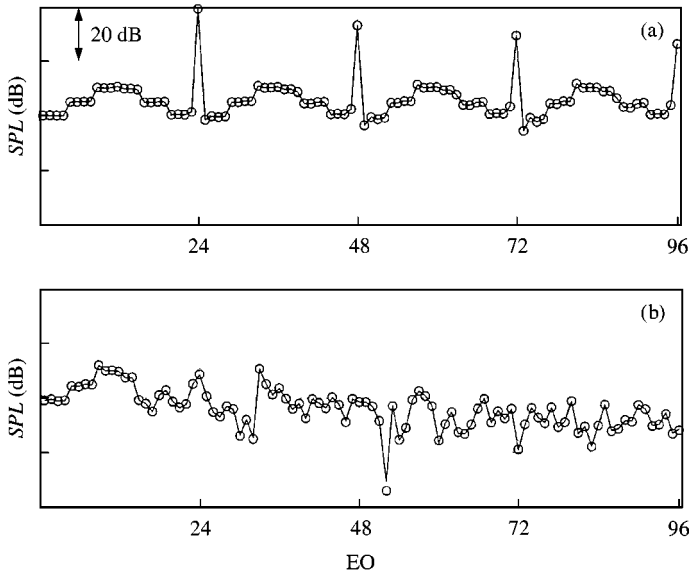

Figure 12. TDNS/FDNS: EO 1–96. Comparison between TDNS results and FDNS results for an example of an irregular sawtooth: (a) near the fan and (b) near the end of the inlet duct. ——, TDNS, ○, FDNS.

A direct comparison between the results for TDNS and FDNS is shown in Figures 11 and 12. Figure 11 shows BPF harmonics 1–4 against T, whilst Figure 12 shows the EO frequency spectrum (a) near the fan and (b) near the end of the inlet duct. The initial

irregular sawtooth constructed to be used in this comparison is similar to the waveforms constructed in section 3.2 for the model FANPAC fan operating at 80% design. (Compare the EO frequency spectrum near the fan in Figures 12(a) and 15(a).)

Provided a large number of harmonics are calculated (with dissipation included in the FDNS model), the two different simulation models generate identical results. These results (when compared with the results in section 3.3) will demonstrate the effect of not including "cut-off" in the model. Note that in Figure 11 the attenuation of the BPF harmonics for an irregular sawtooth is significantly greater than the predictions for a regular sawtooth. Further note that in Figure 12 the amplitude of the low-frequency EO modes remains high by the end of the inlet duct. These observations will be discussed in section 3.3 when compared with results which include "cut-off".

3. RESULTS

3.1. EXPERIMENTAL RESULTS

The experimental results presented in this section were obtained by Rolls–Royce plc during the European Community FANPAC programme. The model fan rig is described by Fisher *et al.* and therefore only brief details of the test programme are repeated in this paper.

The inlet duct is approximately 870 mm in diameter, and contains a "shock track duct" facility which consists of 24 pressure transducers imbedded in the hard-walled cylindrical duct. The transducers were stationed between 13·5 and 594 mm upstream of the fan. Therefore, the aspect ratio of the duct is $L/D \approx 0{\cdot}68$; this is slightly longer than a typical inlet duct where $L/D \approx 0{\cdot}5$.

The fan has 24 blades, and a design speed of 10 100 r.p.m. Results in this paper are for the fan operating at 80, 90 and 98% design (or nominal load NL). At 80% NL the tip speed just exceeds sonic velocity, and hence the "rotor-alone" pressure field will propagate upstream in the inlet duct. The axial station of each transducer may be calculated in terms of T by using equation (1), thereby permitting comparisons between the data and the non-linear simulation models. Comparisons of the attenuation of the first four BPF harmonics with T are presented, and the EO frequency spectrum measured at two positions in the duct which correspond to axial stations where $z/b = 0{\cdot}5$ and 1.

The validity of the weak-shock approximation may be questionable close to the fan. For a regular sawtooth the Sound Pressure Level of the waveform is

$$SPL = 10\log_{10}\frac{\frac{1}{12}p_s^2}{P_{ref}^2}, \tag{25}$$

$$\approx 183{\cdot}2 + 20\log_{10}s \quad \text{at} \quad T = 0, \tag{26}$$

where the static pressure $P_0 = 10^5$ Pa, and the reference pressure $P_{ref} = 20 \times 10^{-6}$ Pa. The amplitude of the BPF tone is approximately 2 dB less than the SPL of the waveform. For example, in Figure 9, the initial BPF tone of $\approx$180 dB corresponds to a shock strength of $s = 0{\cdot}8$. Therefore, although the initial shock strength may be large, the validity of the weak-shock approximation will be reasonable because the shocks are rapidly attenuated (non-linearly) near the fan, thus ensuring that s will then be small.

3.2. SET-UP

The simple plane two-dimensional description of the "rotor-alone" pressure field (Figure 1) is used as the basis for the propagation models: TDNS and FDNS. It is assumed

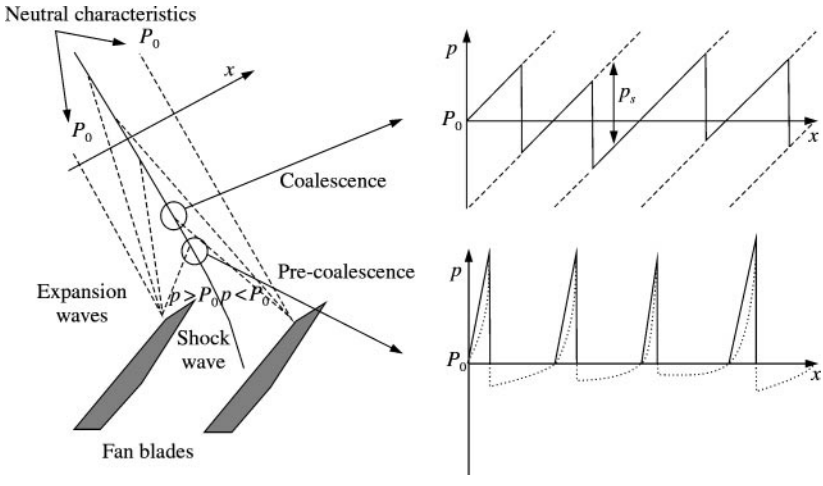

Figure 13. Pressure signature by a supersonic fan.

that shortly upstream of the fan, the shock waves and expansion fans coalesce into a continuous waveform—a sawtooth. The initial conditions for the TDNS and FDNS models are the same; both require the construction of an irregular sawtooth which is representative of the pressure signature near the fan. The subsequent propagation of this waveform from a location near the fan, upstream to the end of the duct, may then be calculated in the time (TDNS) or frequency (FDNS) domain.

The experimental results include EO frequency spectra measured in the inlet duct. These results show the *SPL* by the duct wall at a series of axial stations upstream of the fan. In order to construct an initial waveform, the *SPL* of the BPF tone and the "Buzz-saw" tones near the fan is required. In principle, the "exact" sawtooth may be measured, and this waveform may be used by TDNS and FDNS. However, measuring the sawtooth is in practice difficult because the required data sampling rate must be very high. Therefore, the sawtooth is estimated by using the spectral measurements as outlined below.

There is a small region upstream of the fan before the shock waves and expansion fans coalesce. In this pre-coalescence region the pressure field is assumed to consist of a series of isolated pulses. The true description of the pressure field is undoubtedly more complicated (and the weak-shock approximation will not be valid close to the fan's leading edge). However, this idealized model will provide an instructive description of the generation of an irregular sawtooth.

The idealized pressure signature in the pre-coalescence and coalescence regions is shown in Figure 13. The neutral characteristics are defined to be the expansion waves on which the pressure is equal to P_0. These represent stationary points in the moving frame of reference x. In the pre-coalescence region, perhaps, a realistic pressure signature is shown with the dotted line. The pressure signature is approximated by a series of isolated pulses (shown with the solid line) because it is assumed that the amplitude on one side of the shock (and gradient of the expansion fan) will be far greater than the other side. Hence (by definition), it is assumed that in the pre-coalescence region the majority of the attenuation will be on one side of each shock.

In theory, each isolated pulse may be identified with an individual rotor blade; therefore, the initial amplitude of each pulse may vary slightly to account for variations (pre-dominantly) in the blade stagger angle. The inter-shock spacing λ between the pulses is assumed to be constant because when compared with variations in the blade stagger angle,

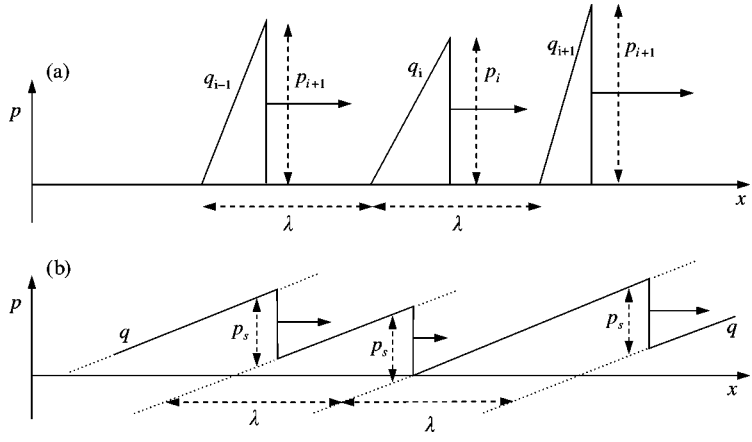

Figure 14. (a) Isolated pulse propagation and (b) irregular sawtooth propagation.

variations in the blade spacing do not significantly contribute to the generation of "Buzz-saw" tones (cf. Stratford and Newby [6]).

In the pre-coalescence region, each shock propagates at a velocity proportional to the shock mid-point pressure p_m (equation (4)), whereas the velocity of each point on the expansion fan is proportional to the pressure at that point (equation (3)). Each shock will coalesce with the preceding expansion fan. If the initial isolated pulses are identical, then each shock will coalesce with the preceding expansion fan at the same time, generating a regular sawtooth. However, if the pulses are not identical, then coalescence between the shocks and expansion fans will occur at slightly different times, thus generating an irregular sawtooth.

During the pre-coalescence region the expansion fans attenuate one side of each shock (because the velocity of a point on the expansion fan close to the top of the shock will travel at a greater velocity than the shock). It is implicitly assumed that the energy dissipated by the shocks is equal to the loss of energy predicted by the non-linear attenuation of each shock. This assumption is discussed in greater detail by Pierce [15] (see pp. 581–582).

By using equation (4) the pressure gradient q of an expansion fan will be

$$q = 1 \Big/ \left(\frac{1}{q(t=0)} + \frac{\gamma + 1}{2\rho_0 a_0} t \right). \tag{27}$$

Assuming $q(t=0) \gg 1$, and by using $a_0^2 = \gamma P_0/\rho_0$ and $T = a_0 t/\lambda$, equation (27) reduces to

$$q(T) \approx \frac{1}{T} \left(\frac{2\gamma P_0}{\gamma + 1} \right) \frac{1}{T}, \tag{28}$$

which is consistent with equation (6). Therefore, after a sufficient time the expansion fans will be linear and independent of their initial gradient. Therefore, differences between the expansion fan gradients attached to each shock become negligible. Denote T_c as the coalescence time (i.e., the time when the last shock and expansion fan have coalesced), and assume that when $T \geqslant T_c$, equations (6) and (28) are valid.

Figure 14(a) sketches a series of isolated pulses equally spaced λ apart with the ith pulse prescribed with shock amplitude p_i and expansion fan gradient q_i. In Figure 14(b), the pulses have all coalesced and the expansion fan gradient q is now the same between each

shock. Therefore, the amplitude of each shock p_s will be the same, although the shock mid-point pressures p_{m_i} will vary.

An irregular sawtooth is constructed by specifying the shock mid-point pressures p_{m_i}, $i = 1 \,..\, B$ at coalescence. Denote the shock with the smallest mid-point pressure, i.e., the shock with the least velocity, and hence the last one to coalesce, by subscript j. Therefore, at coalescence the shock amplitude $p_s(T_c)$ is defined as $2p_{m_j}$, with the expansion fan gradient $q(T_c) = 2p_{m_j}/\lambda$. This will uniquely define an irregular sawtooth specified by the shock mid-point pressures at coalescence.

For a regular sawtooth

$$p_{m_i} = r_0, \quad i = 1 \,..\, B, \tag{29}$$

where r_0 is a constant. For an irregular sawtooth

$$p_{m_i} = r_0 + \sum_{n=1}^{B-1} r_n \sin(2n\pi \mathrm{i}/B - \phi_n), \quad i = 1 \,..\, B, \tag{30}$$

where r_n are constants. The starting level of the BPF tone is prescribed by r_0, and the starting levels of the "Buzz-saw" tones are prescribed by r_n for $n = 1, 2, 3, \ldots$ for EO $1, 2, 3, \ldots$ respectively. The relative phasing of each "Buzz-saw" tone is given by ϕ_n. The relative phasing is unknown, and therefore the phases are generated randomly between $-\pi$ and π. Therefore, the initial waveform constructed at coalescence will not be unique.

However, without the measured data it will be necessary to estimate suitable starting levels for the BPF and "Buzz-saw" tones. In this case, it is suggested that the simplest estimate will be to assume that the initial levels of the "Buzz-saw" tones are all equal. Then only two estimated *SPL*s will be required; namely, the BPF tone and the "Buzz-saw" tone. The initial waveform may be thought as approximately a regular sawtooth with small perturbations in the shock mid-point pressures. Therefore, to estimate the initial BPF tone assume that the waveform is regular, and then the level is calculable in terms of the initial shock strength s (equation (26)). The initial "Buzz-saw" tone level is a measure of the small perturbations in the shock mid-point pressures of the irregular sawtooth. In the Stratford and Newby paper [6] the principle source of perturbations to the pressure signature were due to blade stagger angle variations. In principle, the "Buzz-saw" tone level may be thought of as a function of the blade stagger angle. Stratford and Newby provided an empirical relationship between changes in the blade stagger angle and resulting changes to the pressure signature.

The EO frequency spectrum (EO 1–96) measured at the first transducer in the "shock track duct", for the FANPAC fan operating at 80, 90 and 98% NL, are shown in Figure 15. FDNS predictions were started by using the data measured at the first transducer in the duct in order to construct an initial irregular sawtooth. It is to be emphasized that only the SPL of the BPF and "Buzz-saw" tones is used. Figure 15 shows that the initial frequency spectra of the waveforms generated to be used by FDNS closely resemble the measured data; in particular, there is close agreement between the EO tone levels at frequencies higher than BPF, which suggests that this set-up procedure to construct an irregular sawtooth is realistic.

3.3. FDNS RESULTS

The procedure to construct an initial waveform includes a set of initial phases which are unknown (and therefore generated randomly). Hence, there is no unique waveform constructed at each operating condition. Therefore, a sample of waveforms (which all have

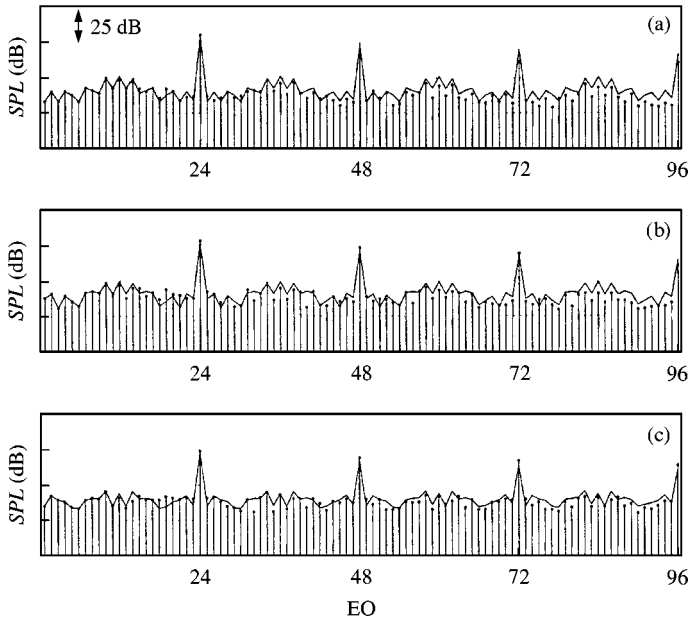

Figure 15. FDNS: EO 1–96. Comparison between FDNS results and experimental data for the FANPAC fan operating at (a) 80, (b) 90 and (c) 98% NL. Spectral comparisons near the fan: —— FDNS; •, FANPAC data.

a frequency spectrum closely resembling the measured spectrum) are generated. Then the non-linear propagation of each waveform is calculated by using FDNS, and the results are then averaged in order to generate a "mean" prediction. At each operating condition the results also include a 95% confidence interval for the sample mean generated by using the student t-test. This provides an estimate of the variation in the results due to small changes in the initial pressure signature caused by changing the phasing whilst constructing the waveform.

Figure 16 shows the variation in the BPF tone for a series of simulations at 90% NL. (The "mean" prediction is shown in Figure 19(a).) At supersonic operating speeds the "Buzz-saw" EO modes facilitate the attenuation of the BPF tone. The BPF tone for a regular sawtooth is attenuated by the transfer of energy between the BPF harmonics. In an irregular sawtooth the BPF tone may also be affected by non-linear interactions between EO modes (other than the BPF harmonics) whose mode numbers' sum or difference equals B, thereby increasing the attenuation of the BPF tone compared with a regular sawtooth. In simple terms, the shock-spacing configuration becomes progressively distorted, and therefore poorly synchronized with the blade passing frequency.

The complexity of the spectral non-linear interactions suggests that prediction of the energy in individual EO modes may be difficult. In theory, there exist shock-spacing configurations which contain little (or no) energy at some of the EO modes. (For example, in a regular sawtooth the Fourier coefficients $C_m \equiv 0$ for all m other than the BPF harmonics.) Whilst the waveform propagates it is continually modified, and hence energy may be transferred to *or* extracted from each EO mode. At some locations in the duct the shock-spacing configuration will become poorly synchronized with an individual EO mode, but because the waveform is continually being modified, the poorly synchronized waveforms are likely to only occur at localized positions in the duct. The attenuation of each tone is therefore not necessarily monotonically decreasing with T. (For example, the

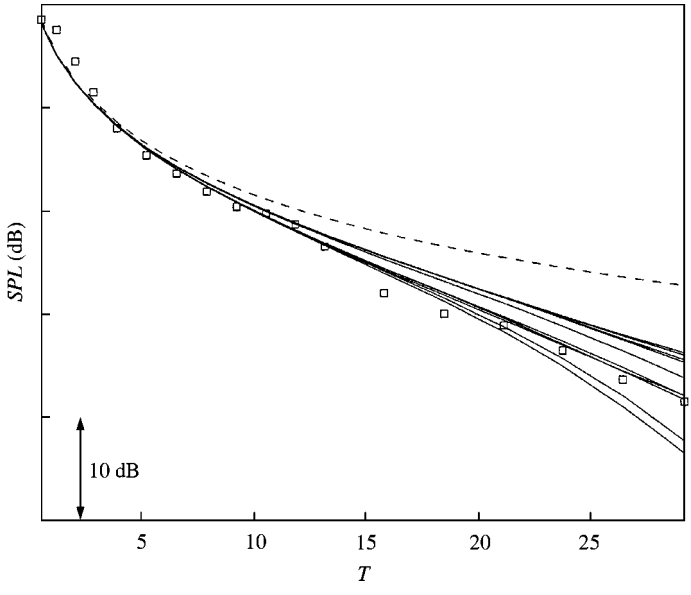

Figure 16. FDNS: variation of BPF tone. Comparison between the theory for a regular sawtooth, FDNS results and experimental data for the FANPAC fan operating at 90% NL: – – –, regular sawtooth; ——— FDNS simulations; □, FANPAC data.

attenuation of the BPF harmonics in Figures 19 and 21 are not all monotonically decreasing.)

In Figure 16, the FDNS simulations vary up to 10 dB by the end of the duct. Hence, the choice of an initial waveform may significantly affect the results. The likelihood of this determines in part the width of the 95% confidence interval bounding the "mean" prediction shown in all the FDNS results. The precise pressure signature generated by a fan is in general unknown. Perturbations in the waveform are primarily caused by small blade-to-blade variations in the fan. These will be different for every fan, even with fans of the same design specification. Therefore, in simplistic terms the measured data may be viewed as the results from a single "observation" for the model fan used in the FANPAC research programme. Whereas the FDNS "mean" predictions may be viewed as the results from a sample of "observations" (generated by numerical simulations) for a set of fans, all with the same design specification as the model fan. Thus, the FDNS results do not represent a precise attempt to predict the experimental data.

Comparisons between the FDNS predictions and experimental data are shown in Figures 17–22 at 80, 90 and 98% NL. Figures 17, 19 and 21 show the first four BPF harmonics against T, for the values of T prescribed over the length of the "shock track duct". Error bars are plotted in these figures to denote the 95% confidence interval. Figures 18, 20 and 22 show the EO frequency spectrum at two axial stations in the inlet duct: $z/b = 0{\cdot}5$ and $z/b = 1$. In these figures, the 95% confidence interval is shown by the dashed lines above and below the "mean" prediction.

In Figure 17, at 80% NL the BPF harmonics are predicted reasonably well by the FDNS simulations. At this speed, there is little difference in the BPF tone between the prediction for a regular sawtooth, the FDNS "mean" prediction, and the experimental data. In Figure 18(b), it is seen that EO modes 1–9 are clearly "cut-off", and that the FDNS results successfully model the decay of these "cut-off" modes. (Compare the amplitudes of these modes by the end of the duct with their starting amplitudes shown in Figure 15(a).) These

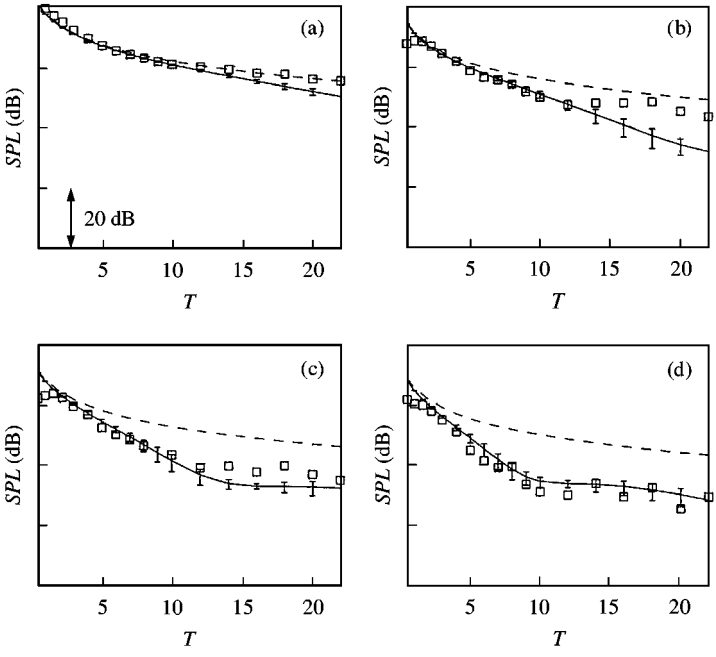

Figure 17. FDNS: BPF harmonics 1–4. Comparison between the theory for a regular sawtooth, FDNS results and experimental data for the FANPAC fan operating at 80% NL: – – –, regular sawtooth; ——, FDNS; □, FANPAC data. (a) 1BPF; (b) 2BPF; (c) 3BPF; (d) 4BPF.

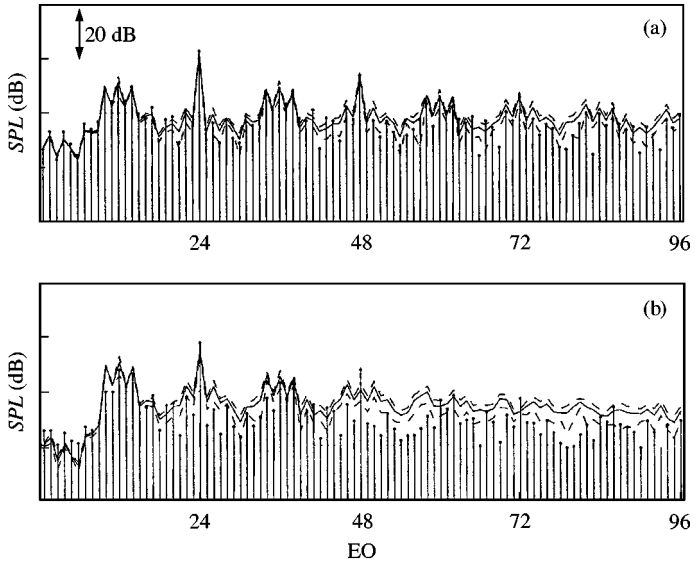

Figure 18. FDNS: EO 1–96. Comparison between FDNS results and experimental data for the FANPAC fan operating at 80% NL: ——, FDNS; •, FANPAC data. (a) $z/b = 0{\cdot}5$; (b) $z/b = 1$.

evanescent modes will have relatively little effect on the other modes in the frequency spectrum.

In section 2.3, Figures 11 and 12 show a comparison between TDNS and FDNS results obtained by using an initial irregular waveform with a frequency spectrum similar to the

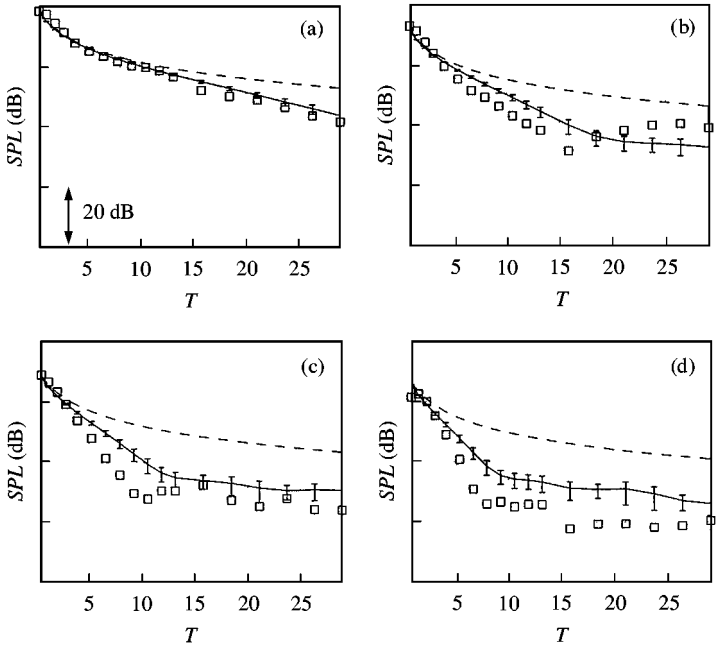

Figure 19. FDNS: BPF harmonics 1–4. Comparison between the theory for a regular sawtooth, FDNS results and experimental data for the FANPAC fan operating at 90% NL: – – –, regular sawtooth; ——, FDNS; □, FANPAC data. (a) 1BPF; (b) 2BPF; (c) 3BPF; (d) 4BPF.

measured spectrum for the FANPAC fan at 80% NL (compare Figures 12(a) and 15(a)). These results when compared with Figures 17 and 18 demonstrate the effect of not including "cut-off" in the model. Firstly, by the end of the inlet duct the attenuation of the "cut-off" EO modes is not predicted. (Compare the EO frequency spectra in Figures 12(b) and 18(b).) By the end of the inlet duct the "Buzz-saw" EO modes will typically be the dominant tones in the EO frequency spectrum. Therefore, close prediction of these tones is desirable. Secondly, as discussed above the presence of high-amplitude "Buzz-saw" EO modes will increase the attenuation of the BPF tone. Therefore, without the inclusion of "cut-off" in the model the amplitudes of *all* the "Buzz-saw" EO modes are likely to remain high by the end of the inlet duct, and this may significantly increase the attenuation of the BPF tone. (Compare the attenuation of the BPF tone in Figures 11(a) and 17(a).) Therefore, predictions generated by using FDNS (with the inclusion of "cut-off" in the model) will in general be a significant improvement over TDNS results.

At 80% NL (compared with 90 and 98% NL) there is less energy in the "Buzz-saw" EO modes (which implies less variation in the shock mid-point pressures), and therefore the sawtooth will be more regular than at the higher speeds. Thus, in Figure 17(a), the attenuation of the BPF tone is predicted closely by the theory for a regular sawtooth. However, at 90 and 98% NL the BPF tone is poorly predicted by the regular sawtooth theory (cf. Figures 19(a) and 21(a)). More low-frequency EO modes will be "cut-off" at 80% compared with those at 90 and 98% NL because 80% is close to the transonic operating speed. Hence, at 80% NL the BPF tone suffers less attenuation by non-linear interactions between modes other than harmonics of BPF, compared with those at higher operating speeds, because there is less energy in the "Buzz-saw" EO modes because of "cut-off". At higher speeds less of these low-frequency "Buzz-saw" EO modes are "cut-off".

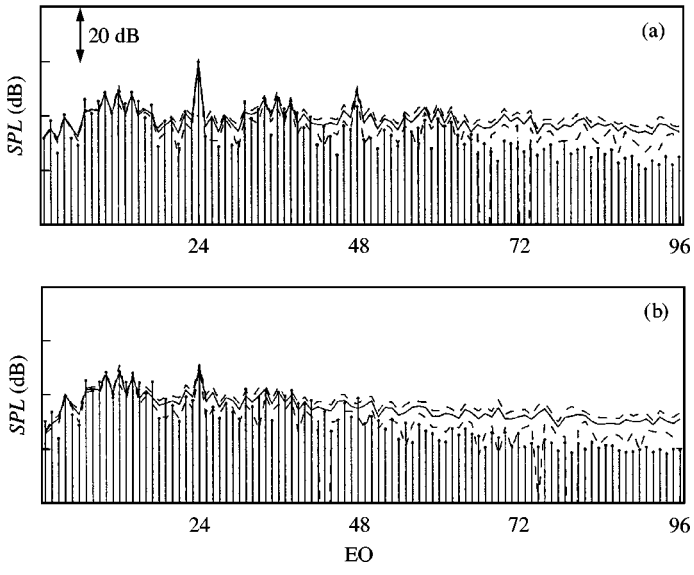

Figure 20. FDNS: EO 1–96. Comparison between FDNS results and experimental data for the FANPAC fan operating at 90% NL: ——, FDNS; •, FANPAC data. (a) $z/b = 0{\cdot}5$; (b) $z/b = 1$.

The EO frequency spectra in Figure 18 show that there is good agreement between the experimental data and the FDNS predictions at 80% NL. At $z/b = 1$, there are three characteristic features in the spectrum to note. Firstly, there are several "Buzz-saw" EO modes which are "cut-off"; including a linear attenuation term in equation (20) has successfully modelled the "cut-off" behaviour. Secondly, the "Buzz-saw" EO modes that are not "cut-off" do not suffer any significant attenuation over the length of the inlet duct. Thirdly, all the high-frequency EO modes ($>$ BPF) are well attenuated by the end of the duct, resulting in a spectrum dominated by the BPF and "Buzz-saw" tones. At this speed these three features have been successfully predicted by the FDNS simulations.

In Figure 19, at 90% NL the first three BPF harmonics are also predicted reasonably well by the FDNS simulations. At this higher operating speed a closer prediction of the BPF tone is obtained by using FDNS, compared with the theory for a regular sawtooth. In Figure 20(b), the dominant energy in the frequency spectrum is in the BPF and "Buzz-saw" tones. Now at most three of the low-frequency EO modes are "cut-off". Once again there is good agreement between the experimental data and the FDNS predictions, but at this speed the close agreement is only observed up to between 2 and $3 \times$ BPF. At higher frequencies the amplitude of the measured data is consistently less than the FDNS "mean" prediction. (Although not significantly less than the lower bound of the 95% confidence interval.)

In Figure 21, at 98% NL the first two BPF harmonics (near the end of the inlet duct) are predicted reasonably well by the FDNS simulations. However, the measured amplitude of each of the BPF harmonics rapidly decays shortly upstream of the fan. The reduction in the BPF tone is greater than 20 dB. This behaviour has not been predicted by the FDNS simulations. This may be caused by a loss of synchronization between BPF and the shock-spacing configuration. However, this behaviour is usually observed further upstream of the fan, presumably because the distortion of the waveform only occurs after a sufficient time (or distance) of propagation. At this high-speed three-dimensional effects will be more significant compared with those at the lower operating speeds, because the shock strength by the duct wall is likely to be reduced at the fan's design condition due to shock

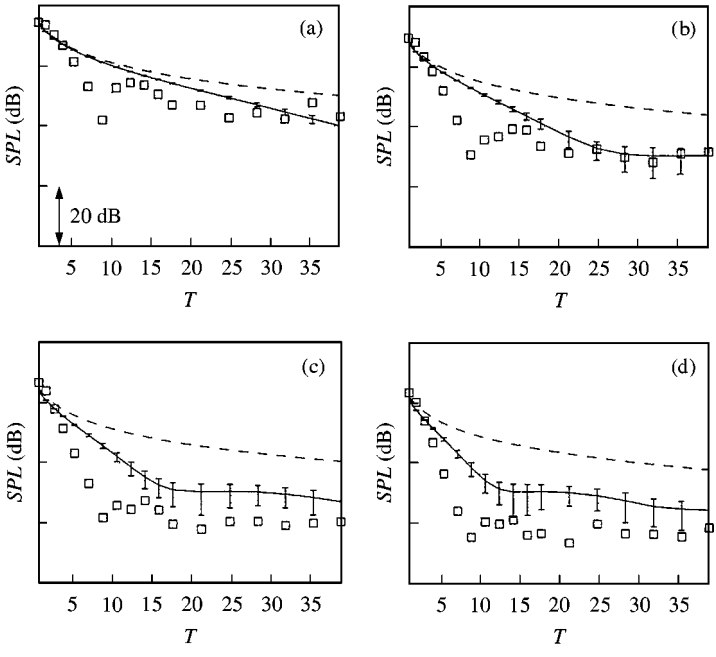

Figure 21. FDNS: BPF harmonics 1–4. Comparison between the theory for a regular sawtooth, FDNS results and experimental data for the FANPAC fan operating at 98% NL: – – –, regular sawtooth; ——, FDNS; □, FANPAC data. (a) 1BPF; (b) 2BPF; (c) 3BPF; (4) dBPF.

swallowing. (Note in Figure 15(c) the measured BPF tone near the fan is less than at 80 and 90% NL.) Also, it is plausible that there may be destructive interference between the first and second ($n = 1, 2$) radial modes close to the duct wall. At this speed, all the higher order radial modes may not be "cut-off". The radial eigenfunctions prescribed by the Bessel functions J_m with $n = 1$ and 2 have opposite signs at the duct wall. There is no radial dependence prescribed in the FDNS model, and therefore the rapid decay of the BPF tone close to the fan may not be possible to predict by using this simulation model. However, from a practical point of view this speed is not an important operating condition for noise.

In Figure 22(b), the dominant energy in the frequency spectrum is again in the BPF and "Buzz-saw" tones. Now at most one of the low-frequency EO modes is "cut-off". Once again there is good agreement between the experimental data and the FDNS predictions, but at this speed the close agreement is only up to about $2 \times$ BPF. At higher frequencies the amplitude of the measured data is again consistently closer to the lower bound of the 95% confidence interval than the FDNS "mean" prediction.

In general, the dominant energy in the frequency spectra at 90 and 98% NL are the "Buzz-saw" tones, and their level has been successfully predicted by the FDNS simulations (cf. Figures 20 and 22). At these higher speeds fewer of the "Buzz-saw" EO modes are "cut-off". The amplitude of the "Buzz-saw" tones remains approximately constant in the inlet duct. It is believed that the high-frequency ($>$ BPF) EO modes are more efficiently attenuated compared with the low-frequency ($<$ BPF) EO modes (particularly at these high operating speeds), and therefore there is no mechanism to enable the attenuation of these "Buzz-saw" tones. (Non-linear spectral interactions between the low- and high-frequency modes will not occur because the high-frequency modes are rapidly attenuated to linear amplitudes.) The comparison between the data and FDNS is poorer at high frequencies at

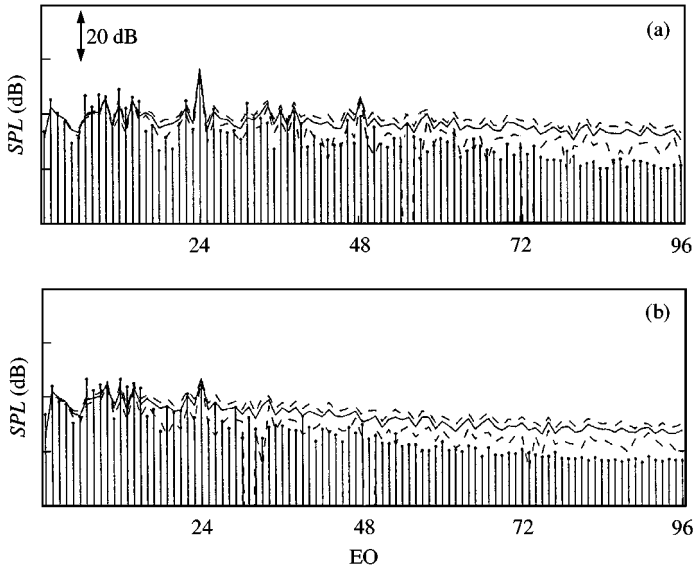

Figure 22. FDNS: EO 1–96. Comparison between FDNS results and experimental data for the FANPAC fan operating at 98% NL: ——, FDNS; •, FANPAC data. (a) $z/b = 0{\cdot}5$; (b) $z/b = 1$.

both 90 and 98% NL. It is also noted that the measured amplitude of the high-frequency EO modes at 90 and 98% NL is significantly less than at 80% NL.

The dissipation of energy by the shocks has not been examined in this paper. In TDNS energy dissipation is not explicitly included in the formulation of the model. In FDNS, energy dissipation is explicitly included, *but* not to directly model the dissipation of energy by the shocks. It is sufficient in this paper to assume that the dissipation of energy by the shocks will be more efficient at high frequencies; this behaviour is formulated by the diffusion term in Burgers equation (19), although in the FDNS model it is included to necessarily dissipate energy at the high frequencies close to the truncation point of the Fourier series. The rate of attenuation of the high-frequency EO modes is therefore questionable, and in particular at 90 and 98% NL there is not such close agreement between the data and the predictions at the high frequencies compared with those at the low frequencies.

4. CONCLUSIONS

The "rotor-alone" pressure field in the inlet duct of an aero-engine is approximated by a plane two-dimensional model consisting of a series of shock waves and expansion fans, generated by a uniform supersonic flow impinging on a cascade of fan blades. The shock waves and expansion fans coalesce generating a pressure signature, which in a direction normal to the shocks, is characteristically a sawtooth waveform. This model approximates the "rotor-alone" pressure field attached to a supersonic ducted rotor inside an aero-engine inlet duct.

By assuming the shocks are "weak", the attenuation of a regular sawtooth is predicted by using weak-shock theory. Similarly, the propagation of an irregular sawtooth is calculated in the time domain by using weak-shock theory. However, this model (TDNS) does not include the effect of the duct wall on the pressure waveform. In most modern aero-engines

there will be an acoustic liner on the wall of the inlet duct. However, in a hard-walled inlet duct there will be a range of modes (or frequencies) that are "cut-off". An alternative model (FDNS) is developed which approximates the inherently three-dimensional duct wall boundary condition in a two-dimensional model. The problem is transformed into the modal/frequency domain, and the attenuation of modes with frequencies up to $100 \times$ BPF is calculated. The inclusion of a numerical diffusion term enables the Fourier series to be truncated without adversely affecting the results. This model will be applicable to use with both hard- and soft-walled inlet ducts. In this paper, results are presented for hard-walled ducts only.

In a subsequent paper the effect on "Buzz-saw" tone generation with soft-walled inlet ducts will be discussed. A similar analytic expression for the non-linear attenuation of a regular sawtooth in the presence of an acoustic liner is known [8, equation 2.11]. In a soft-walled inlet duct the liner performance will depend on the mode number (or frequency), and the operating speed of the fan. These may both be incorporated into the FDNS model. With a hard-walled inlet duct the linear attenuation term which is used to modify Burgers equation is only an absorption term (i.e., in equation (20) σ is real). However, in equation (8) k_z is complex, and with an acoustic liner, it will be more realistic to set σ to be complex in order to include the effect on the phase caused by the liner, in addition to the attenuation.

Finally, the noise radiated from the inlet duct of an aero-engine may not be confined to the "rotor-alone" noise. In practice, the inlet flow will not be uniform, and the non-uniform inlet flow may generate noise commonly known as "distortion" or "interaction" tones (closely analogous to rotor–stator interaction tones). The experimental data does not differentiate between the alternative noise sources. Therefore, the results in this paper also suggest that in a hard-walled inlet duct the dominant noise source is the "rotor-alone" pressure field.

ACKNOWLEDGMENTS

The authors wish to thank Dr R. H. Self (ISVR) for his contribution during the period of this work, and in particular for his suggestion regarding the use of dissipation in the FDNS model. The authors also wish to acknowledge the contributions of Mr J.-M. Buchmann and Dr D. A. K. Hewlett (both formerly at the ISVR) during the early stages of this work (in particular, for their development of the TDNS code). We also thank Professor C. L. Morfey (ISVR) for his comments on this work.

We also wish to thank Dr B. J. Tester and Mr P. J. G. Schwaller (Rolls–Royce plc) for their assistance and valuable technical discussions during the period of this work, and for the provision of experimental data from the European Community FANPAC research programme.

The work was funded by the European Community research projects RESOUND and DUCAT. The support of Mr P. Kruppa (Technical Monitor for the Commission) is particularly acknowledged.

One of us (MJF) wishes to acknowledge the continuing financial support provided by Rolls-Royce plc.

REFERENCES

1. M. G. PHILPOT 1970 *ASME Paper No.* 70-*GT*-54. The Buzz-saw noise generated by a high duty transonic compressor.

2. D. L. HAWKINGS 1971 *Journal of Sound and Vibration* **17**, 241–250. Multiple tone generation by transonic compressors.
3. M. KUROSAKA 1971 *Journal of Sound and Vibration* **19**, 453–462. A note on multiple pure tone noise.
4. M. R. FINK 1971 *ASME Paper No.* 71-*GT*-7. Shock wave behaviour in transonic compressor noise generation.
5. G. F. PICKETT 1972 *Journal of Aircraft* **9**, 658–663. Prediction of the spectral content of combination tone noise.
6. B. S. STRATFORD and D. R. NEWBY 1977 *AIAA* 77-1343. A new look at the generation of Buzz-saw noise.
7. C. L. MORFEY and M. J. FISHER 1970 *The Aeronautical Journal of the Royal Aeronautical Society* **74**, 579–585. Shock-wave radiation from a supersonic ducted rotor.
8. M. J. FISHER, B. J. TESTER and P. J. G. SCHWALLER 1998 *AIAA* 98-2249. Supersonic fan tone noise prediction.
9. W. EVERSMAN 1991 in *Aeroacoustics of Flight Vehicles*: *Theory and Practice*, Vol. 2, *Noise Control NASA RP*-1258, 101–163. Theoretical models for duct acoustic propagation and radiation.
10. D. G. CRIGHTON 1979 *Annual Reviews of Fluid Mechanics* **11**, 11–33. Model equations of nonlinear acoustics.
11. G. B. WHITHAM 1974 *Linear and Nonlinear Waves*. New York: John Wiley & Sons, Inc.
12. D. G. CRIGHTON, A. P. DOWLING, J. E. FFOWCS WILLIAMS, M. HECKL and F. G. LEPPINGTON 1992 *Modern Methods in Analytical Acoustics*. New York: Springer.
13. F. H. FENLON 1971 *Journal of the Acoustical Society of America* **50**, 1299–1312. A recursive procedure for computing the nonlinear spectral interactions of progressive finite-amplitude waves in nondispersive fluids.
14. A. KORPEL 1980 *Journal of the Acoustical Society of America* **67**, 1954–1958. Frequency approach to nonlinear dispersive waves.
15. A. D. PIERCE 1989 *Acoustics*: *An Introduction to its Physical Principles and Applications*. New York: Acoustical Society of America.